Supplementary materials for

On the role of the south Pacific subtropical high at the onset of El Niño events

METHODS

Wind Equator. In contrast to the Trade winds in the Atlantic Ocean, the Trade Winds in the Pacific Ocean are symmetric about the ~5 °N -~8 °N of latitude, rather than the geographic equator (**Extended Data Fig.1a-b**). This is confirmed by **Sailing Directions**[26] and **Routeing Chart 5127** (2012) published by UK Hydrographic Office (**Extended Data Fig.2**), suggesting that the NE Trade Winds may divert to NW or westerly once crossing the ~5 °N -~8 °N of latitude. This can explain why the westerly winds can be seen in north of the equator in the western equatorial Pacific during El Nino events. The seasonal southward shifts of the Trade Winds are considered to be able to induce westerly winds during non-El Nino periods due to the elliptical shape of the SPSH but not sufficient to trigger El Nino events, rendering the occurrences of the westerly winds during non-El Nino periods more plausible.

The superposition of the NW or westerly winds onto a southward shift of the SPSH pushes the ECC eastward and southward to the geographic equator or more south, bringing the giant pool of the warm waters to the central and the eastern equatorial Pacific, thus leading to SSTs anomalies. The weakening of the SE Trade Winds due to southward migrations of the SPSH allows for a wide southward extension of the westerly wind fetch (**Extended Data Fig.1b**). The magnitude of the westerly wind fetch is determined by the meridional position of the SPSH.

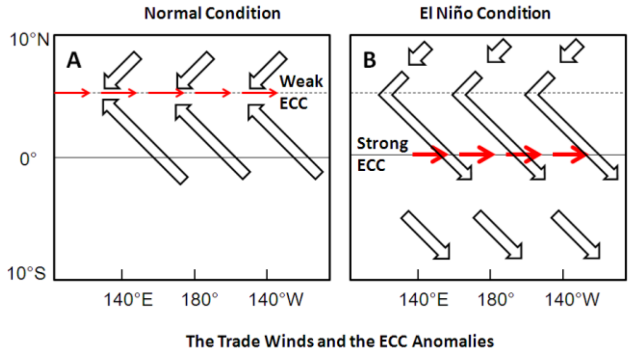

Extended Data Fig 1. Schematic plots for the Trade Winds and the ECC anomalies. A, The Trade Winds and the ECC in normal condition. The Trade Winds are symmetric about ~5 °N -~8 °N of latitude (see Sailing Directions and Routeing Chart 5127 published by UK Hydrographic Office in 2012). The climatologically mean axis of the ECC is at about ~5 °N -~8 °N with weak intensity. **B,** The Trade Winds and the ECC in El Niño condition. The Trade Winds change the direction from NE to NW after crossing the wind equator (about ~5 °N -~8 °N). The mean axis of the ECC is at about ~0 ° with strong intensity**.** The hollow arrows and solid red arrows represent the Trade Winds and the ECC, respectively.

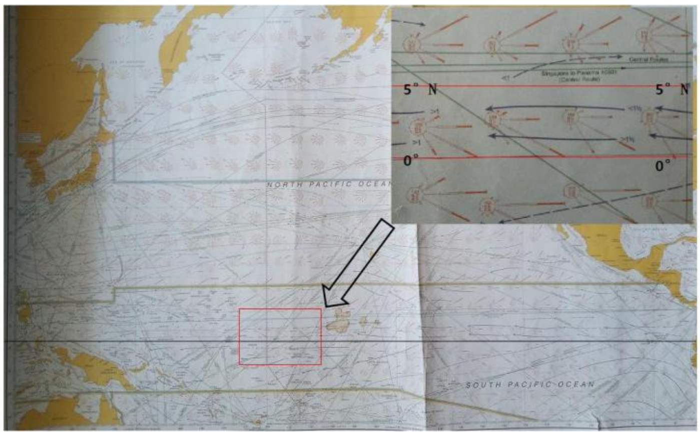

Extended Data Fig 2. Routeing Chart 5127 (July) published by UK Hydrographic Office in 2012. The wind roses in pink color indicate the direction, intensity and frequency of the Winds. The intensity of the winds from any direction is given by the thickness of the staff while the frequency is given by the length of the staff. The inlet map is a large scale of the square in red color, showing a frequency of ~40%-50% SE Trade Winds (~45% Easterly) in July between ~0 °N ~5 °N in the middle of the Pacific. More details in text can be found in **Sailing Directions**.

Coupled Model. The model adopted in this study is a slightly modified version of Lengaigne et al. (2006), with an intermediate complex climate GCM, HadOPA, coupling the OPA ocean model and the HadAM3 atmospheric model through OASIS 2.4. The OPA model consists of the global configuration ORCA (Madec et al., 1998) (also see documentation at http:// www.lodyc.jussieu.fr/opa/). This model has a horizontal resolution of 2 ° both in latitude and longitude with a refinement to 0.5 ° in the meridional direction near the equator, and has 31 levels in the vertical. The vertical grid spacing increases smoothly from 10 m at the surface to about 50 m near 500 m, about 70 m near 1000 m depth, and about 400 m at 6000 m.

The model uses a free surface formulation (Roullet and Madec, 2000). Vertical eddy viscosity and diffusivity coefficients are computed from a 1.5 turbulent closure scheme (Blanke and Delecluse, 1993) allowing an explicit formulation of the mixed layer as well as a minimum diffusion in the thermocline. Horizontal viscosity is of Laplacian type and lateral diffusivity is ‘‘quasi-pure’’ isopycnal as described in Guilyardi et al. (2001). There is no interactive sea-ice model in this configuration: sea-ice cover is relaxed towards observed monthly climatology.

This OGCM has been extensively validated in uncoupled mode in the tropics where it closely matches the observations (Vialard et al., 2001; Lengaigne et al., 2003). In particular, the model succeeds in reproducing the basin wide structures of currents and sea level and temperature, and accurately simulates the Kelvin waves (Lengaigne et al., 2002), of particular importance for the current study. This model is also widely used in coupled mode for process studies (Guilyardi et al., 2001; Guilyardi et al., 2003; Inness et al., 2003), paleoclimate simulations (Braconnot et al., 1999) and climate change experiments (Friedlingstein et al., 2001).

The HadAM3 atmospheric model has different horizontal resolutions in latitude and longitude. The resolution of 2.5° by 3.75° can best meet the requirements of the simulations. The 19 vertical levels, corresponding to a layer thickness of about 100 hPa in the mid-troposphere, are evenly spacing in the lower levels but are smaller near the boundary layer and around the tropopause. Convection is parameterized using the mass-flux scheme of Gregory and Rowntree (1990), with the addition of convective momentum transport (Gregory et al., 1997). A more detailed description of this model and its performance in atmospheric model intercomparison project (AMIP)-type integrations can be found in Pope et al. (2000) and references therein. The HadAM3 has also been performed and tested by Inness et al. (2001) to simulate aspects of tropical intraseasonal activity, in well agreement with the observations.

The ocean is coupled with the atmospheres via the air-sea fluxes and SST exchange through OASIS 2.4 (Valke et al., 2000). Air-sea fluxes and SST are exchanged every day.

It is worth noting that the SPSH advances southwesterly with an intensifying in austral summer and retreats northeasterly with a weakening in austral winter in seasonal cycle. However, the SPSH shifts southwestward with a weakening during El Nino periods and migrates northeastward with an intensifying during La Nina, suggesting that the intensity of the SPSH play a negligible role (the seasonal intensifying of the SPSH offsets the El Nino-related weakening of the SPSH in austral summer).

In order to account for the low-frequency modulation of the wind stress curls (WSC) by the meridional position of the SPSH, a simplified scheme of coupled WSC-SPSH relationship is applied (He et al., 2004). The intensity of the ECC is linearly related to the reversed Walker Circulation which is determined by the veered NE Trade Winds and the MJO-related westerly winds. The meridional position of the ECC, however, is automatically calculated based on the relationship between the ECC and the wind stress curls and the SPSH obtained by running this model with persistent appropriate background forcings (Shchepetkin and Mcwilliams, 2005) (**Extended Data Fig.5**). The relationship of a coupled SST-WSC is also employed (Lian et al., 2014). The initial longitude of the westerly winds is set to 150°E (the area in west of the 150°E is largely influenced by the regional circulations), with a magnitude of 0.08 Nm^{-2}. In contrast to Lengaigne et al. (2006) who used strong westerly winds to simulate El Ninos, only weak westerly winds are needed to produce strong SST anomalies in Nino3 region after applying the relationship of a coupled ECC-SPSH to this study. The initial triggering of the MJO-related westerly winds is purely random, but it is allowed to actually occur only when the meridional position anomalies of the ECC exceed +3°. For simplicity, the veered NE Trade Winds are considered same with the MJO-related westerly winds. The mean meridional position of the ECC is set to 5°N in winter and 8°N in summer (climatological mean). The mean min/max meridional position of the SPSH is set to 16°S/35°S and the mean min/max zonal position of the SPSH is set to 105°W/80°W (climatological mean). The mean position of the Peru Current is set to be linearly related to the merional position of the SPSH. The SPSH moves northerly or southerly (constrained latitudes 10°S-48°S) at a speed of 0.17° per day, which is representative of the observed shifting speed. Once above conditions are met, The meridional position and intensity of the ECC, westerly winds, NE/SE Trade Winds, upwelling feedbacks, SSTs anomalies, etc., will follow the variations of the SPSH. The surface mixed layer of the model is fixed to 50 m, and the mixed-layer heat budget, including all components of anomalous advection and a linear damping, is a standard output of the model. This simulation covers the evolution over a two-year period. We define that a southward shift of the SPSH is weak as $\Delta\varphi_{spsh}$ is less than 7° with a speed of 0.15° per day or less while a southward shift of the SPSH is strong as $\Delta\varphi_{spsh}$ is great than 9° with a speed of 0.3° per day or more.

The SST data used in this study is the Hadley Centre Global Sea Ice and Sea Surface Temperature (HadISST) version 1.1 from 1961 to 2010 with a resolution of 1° by 1° (http://www.metoffice.gov.uk/hadobs/hadisst/data/download.html). The daily surface wind speed is from the National Centres for Environmental Prediction (NCEP) reanalysis from 1961 to 2010 with a resolution of 2.5° by 2.5° (http://www.esrl.noaa.gov/psd/data/gridded/data.ncep.reanalysis.surface.html). The warm-water volume, which is defined as the integral of water above the 20℃

isotherm over the equatorial Pacific (120°E to 80°W, 5°S to 5°N) (Meinen and McPhaden, 2000), is derived from the potential temperature and salinity datasets from the NCEP Global Ocean Data Assimilation System (GODAS) reanalysis from 1980 to 2014 (http://www. esrl.noaa.gov/psd/data/gridded/data.godas.html).

Although the simulated zonal wind stress and ECC position anomalies are relatively in agreement with the observations (**Fig 5. & Extended Data Figs 5-6**), the model overestimates the maximum SST anomalies by about 10% due to a relatively simplified structure.

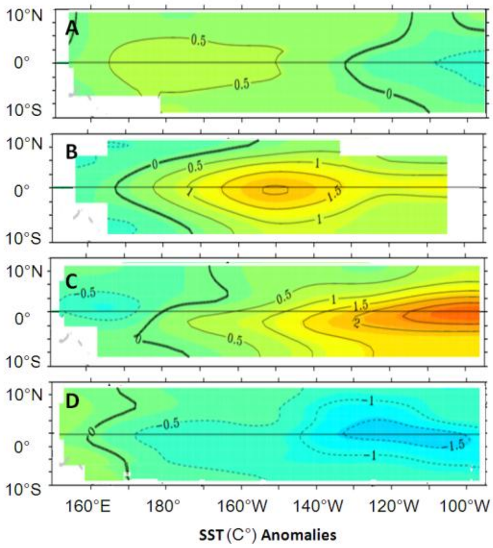

Extended Data Fig 3.**Simulated El Niños and La Nina. A,** a CP-El Niño (weak) near the dateline as the $\Delta\varphi_{spsh}$ is ~+7 °of latitude (a southward anomaly is positive). **B,** a canonical El Niño between central and the eastern tropical Pacific as the $\Delta\varphi_{spsh}$ is ~+8 °of latitude. **C,** an EP-El Niño in the eastern tropical Pacific as the $\Delta\varphi_{spsh}$ is ~+9 °of latitude. **D,** a weak La Niña near the eastern tropical Pacific as the $\Delta\varphi_{spsh}$ is ~ -2° of latitude with zonal position anomalies ($\Delta\lambda_{spsh}$) ~ +5 °of longitude (an eastward anomaly is positive).

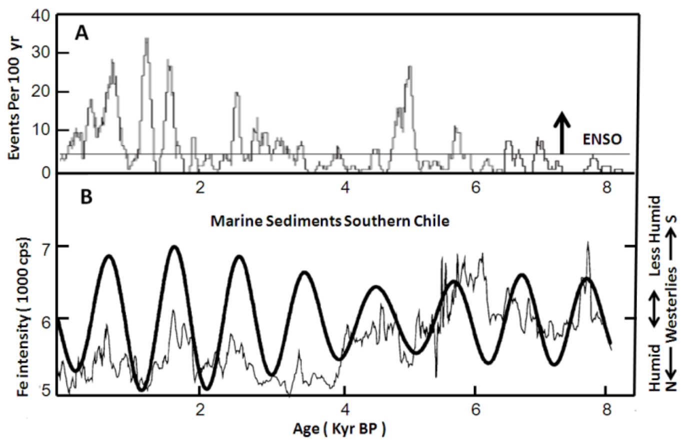

Extended Data Fig 4. Comparison between changes in ENSO variability and the variations of the iron concentrations which are thought to reflect the position shifts of the Westerlies off southern Chile during the Holocene. **A**, Previously published time series and wavelet power spectrum documenting the number of ENSO events in 100-yr overlapping windows during the Holocene (Moy et al., 2002). **B**, Previously published iron content of marine sediments off southern Chile is interpreted as a proxy for rainfall and the position of the Southern Westerlies (thinner line=five-point moving average) (Varma et al., 2011).

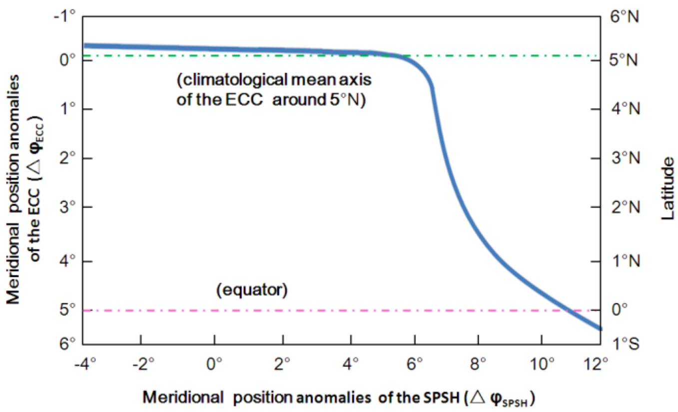

Extended Data Fig 5. The response of the meridional position anomalies of the ECC to the meridional position anomalies of the SPSH. A southward position anomaly is positive. The dashed green line and pink line represent the climatological mean axis position of the ECC and the equator position, respectively.

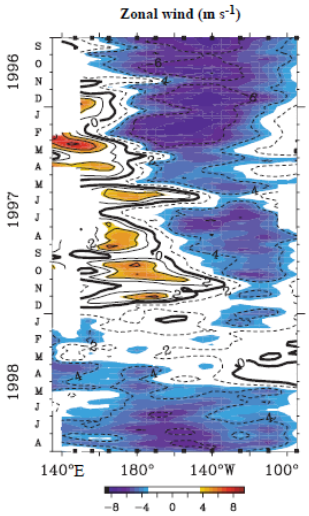

Extended Data Fig 6. Surface zonal wind from September 1996 to August 1998. Analyses are based on 5-day averages for between 2°N and 2°S for the TAO data. Positive winds are westerly, negative winds are easterly (McPhaden, 1999).

Supplementary references and notes

Blanke B, Delecluse P. Variability of the tropical Atlantic ocean simulated by a general circulation model with two different mixed layer physics. *J Phys Oceanogr* **23**, 1363-1388(1993).

Braconnot P, Joussaume S, Marti O, de Noblet N. Synergistic feedback from ocean and vegetation of the African monsoon response to mid-Holocene insolation. Geophys Res Lett 26, 2481–2484 (1999).

Friedlingstein P, Bopp L, Ciais P, Dufresne J-L, Fairhead L, LeTreut H, Monfray P, Orr J. Positive feedback between future climate change and the carbon cycle. Geophys Res Lett 28, 1543-1546(2001).

Gregory D, Rowntree PR. A mass flux convection scheme with the representation of cloud ensemble characteristics and stability dependent closure. Mon Wea Rev 118, 1483-1506 (1990).

Gregory D, Kershaw R, Inness PM. Parametrisation of momentum transport by convection II: tests in single column and general circulation models. Q J R Meteor Soc 123, 1153-1183(1997).

Guilyardi E, Delecluse P, Gualdi S, Navarra A. Mechanisms for ENSO phase change in a coupled GCM. J Climate 16, 1141-1158 (2003).

Guilyardi E, Madec G, Terray L. The role of lateral ocean physics in the upper ocean thermal balance of a coupled oceanatmosphere GCM. Clim Dyn 13, 149-165(2001).

He, R., Liu, Y.& Weisberg, R. H Coastal ocean wind fields gauged against the performance of an ocean circulation model. Geophys Res Lett 31(14), 189-207(2004).

Inness P, Slingo JM, Guilyardi E, Cole J. Simulation of the Madden-Julian oscillation in a coupled general circulation model II: the role of the basic state. J Climate 16, 365-382 (2003).

Inness PM, Slingo JM, Woolnough SJ, Neale RB, Pope VD. Organization of tropical convection in a GCM with varying vertical resolution: implications for the simulation of the Madden-Julian oscillation. Clim Dyn 17, 777-793 (2001).

Lengaigne M, Madec G, Menkes C, Alory G. The impact of isopycnal mixing on the tropical ocean circulation. J Geophys Res 108, 3345. DOI 10.1029/2002JC001704(2003b).

Lengaigne M, Boulanger J-P, Menkes C, Masson S, Madec G, Delecluse P. Ocean response to the march 1997 westerly wind event. J Geophys Res 107, DOI 1029/2001JC000841(2002).

Lian, T., Chen, D., Tang, Y. & Wu, Q. Effects of westerly wind bursts on El Nino: A new perspective. Geophys Res Lett 41, 3522–3527 (2014).

Madec G, Delecluse P, Imbard M, Le′vy C. OPA 8.1 Ocean general circulation model reference manual. Note du Po ˆ le de mode′ lisation, Institut Pierre-Simon Laplace. No. 11, pp 91(1998).

Meinen, C. S. & McPhaden, M. J. Observations of warm water volume changes in the equatorial Pacific and their relationship to El Nino and La Nina., J. Clim 13, 3551–3559 (2000).

Pope VD, Gallani ML, Rowntree PR, Stratton RA. The impact of new physical parametrisations in the Hadley Centre climate model-HadAM3. Climate Dyn 16,

123-146(2000).
Roullet G, Madec G. Salt conservation, free surface and varying volume: a new formulation for Ocean GCMs. J Geophys Res 105, 23927-23942(2000).
Shchepetkin, A. F. & Mcwilliams, J. C. The regional oceanic modeling system (ROMS): a split-explicit, free-surface, topography-following-coordinate oceanic model. Ocean Modelling 9(4), 347-404 (2005).
UK Hydrographic Office. Routeing Chart 5127, Taunton, UK (2012).
Valke S, Terray L, Piacentini A. The OASIS coupled user guide version 2.4, Technical Report TR/ CMGC/00-10, CERFACS (2000).
Vialard J, Menkes C, Boulanger J-P, Delecluse P, Guilyardi E, McPhadenet MJ, Madec G. Oceanic mechanisms driving the SST during the 1997-1998 El Nino. J Phys Oceanogr 31, 1649-1675(2001).
http://www.esrl.noaa.gov/psd/data/gridded/data.ncep.reanalysis.surface.html
http://www. esrl.noaa.gov/psd/data/gridded/data.godas.html
http://www.metoffice.gov.uk/hadobs/hadisst/data/download.html